$La_2SrCr_2O_7$: Controlling the tilting distortions of n = 2 Ruddlesden-Popper phases through A-site cation order.

Ronghuan Zhang, Brian M. Abbett, Gareth Read, Franz Lang, Tom Lancaster, T. Thao Tran, P. Shiv Halasyamani, Stephen J. Blundell, Nicole A. Benedek, and Michael A. Hayward

Supporting Information

1. Structural models refined against the neutron powder diffraction data.
   Figure S1. Observed, calculated and difference plots from the structural refinement of $La_2SrCr_2O_7$ against neutron powder diffraction data collected at room temperature. Lower tick marks indicate peak positions for the majority phase, upper tick marks for the $LaCrO_3$ secondary phase.
   Table S1. Selected bond lengths from the refined structure of $La_2SrCr_2O_7$ at 298K.

2. A-Cation displacements in $La_2SrCr_2O_7$ structural models.
   Figure S2. Structures of $La_2SrCr_2O_7$ refined in space groups $A2_1am$ and A2/a. Arrows indicate the displacement of the (La/Sr) A-cation sites from the high symmetry positions.

3. Magnetic Symmetry Analysis.

4. Magnetic refinement details.
   Table S2. Nuclear and magnetic structural parameters refined against neutron powder diffraction data collected at 5 K from $La_2SrCr_2O_7$.
   Figure S3. Observed, calculated and difference plots from the structural refinement of $La_2SrCr_2O_7$ against neutron powder diffraction data collected at 5K. Lower tick marks indicate nuclear peak positions for the majority phase, middle tick marks for the $LaCrO_3$ secondary phase, upper tick marks magnetic peak positions for the majority phase.

5. μ^+SR data

   Figure S4. Oscillations in the asymmetry of μ^+SR data collected from $La_2SrCr_2O_7$ at low temperature indicate long range magnetic order, consistent with the observation of antiferromagnetic order in the phase via neutron powder diffraction.

6. First principles structures.
   Table S3. Symmetries of the structures we considered with alternate A-site orders. Refer to Figure S5. For labelling scheme of the La and Sr sites.
   Figure S5. Schematic labelling the A-site positions.
   Figure S6. Relaxed energies per formula unit (f.u.) of our 108 structures with varying La/Sr distributions with respect to the energy of the *Amam* reference structure with La/Sr cations on their expected sites (we take the energy of this structure to be the zero of energy, indicated by the horizontal dashed line). Color and shape of points indicate the ratio of Sr/La distribution and initial ionic positions respectively. The horizontal axis is the mean

distance between Sr cations in our relaxed *Amam* structure after swapping Sr/La positions, but before any further relaxation.

7. Magnetic ordering in first principles calculations
   Figure S7. Calculated energies of our relaxed structures. The zero of energy is taken as the energy of the Amam structure with ferromagnetic spin ordering. Colored points have ferromagnetic ordering, while the corresponding gray point is the energy of the same structure with antiferromagnetic ordering.

8. Linear correlation analysis of structural features
   Table S4. List of the structural features we calculated for each of our relaxed structures.
   Figure S8. Linear correlation coefficients of the features listed in Table SX2 for structures relaxed starting from A2/a ionic positions and constrained to the experimental unit cell.
   Figure S9. Linear correlation coefficients of the features listed in Table SX2 for structures relaxed starting from A2/a ionic positions with the unit cell fully relaxed.

1. Structural Models

All the structural models refined against the neutron powder diffraction data were based on the symmetry analysis by Aleksandrov and Bartolome (*J. Phys.:Condens. Matter* **1994**, *6*, 8219-8235). All models were constructed as a' = √2×a, b' = √2×b, c' = c expansions on the highest symmetry I4/mmm description of the undistorted $A_3B_2O_7$ structure. The lattice vector orientation was conserved between different symmetry descriptions, necessitating the use of non-standard space group settings as detailed below. Outline descriptions of each of the models are described below.

***Acam* #64 ($00\Psi_z/00\Psi_z$)**

Atom	Wycoff	x	y	z
La/Sr	4b	½	0	0
La/Sr	8d	½	0	~ 0.18
Cr	8d	0	0	~ 0.09
O	4a	0	0	0
O	8d	0	0	~0.19
O	16g	¼ + x	¼ + y	~0.1

***Acaa* #68 ($00\Phi_z/00\Phi_z$)**

Atom	Wycoff	x	y	z
La/Sr	4b	¾	¼	0
La/Sr	8e	¾	¼	~ 0.18
Cr	8e	¾	¾	~ 0.09
O	4a	¾	¾	0
O	16i	½ + x	½ + y	~ 0.09
O	8e	¾	¾	~ 0.19

***Acmm* #67 (ΦΦ0/-Φ-Φ0)**

Atom	Wycoff	x	y	z
La/Sr	4g	¼ +x	¾	0
La/Sr	8n	¼ + x	¼	~ 0.31
Cr	8n	¾ + x	¼	~ 0.4
O	8n	¼ + x	¾	~ 0.7
O	4g	¾ + x	¼	½
O	8i	½	½	~ 0.1
O	8h	0	½	~ 0.1

***Amam* #63 (ΦΦ0/ΦΦ0)**

Atom	Wycoff	x	y	z
La/Sr	4c	¼	¼ + y	½
La/Sr	8g	¾	¼ + y	~ 0.18
Cr	8g	¼	¼ + y	~ 0.09
O	8g	¼	¼ + y	~ 0.20
O	4c	¼	¼ + y	0
O	8e	½	0	~ 0.09
O	8e	0	½	~ 0.09

***Amam disordered* #63 (ΦΦ0/ΦΦ0)**

Atom	Wycoff	X	y	z
La/Sr	4c	¼	¼ + y	½
La/Sr	8g	¾	¼ + y	~ 0.18
Cr	8g	¼	¼ + y	~ 0.09
O	8g	¼	¼ + y	~ 0.20
O	4c	¼	¼ + y	0
O*	16h	½ + x	y	~ 0.09
O*	16h	x	½ + y	~ 0.09

* occupancy = 1/2

***A2$_1$am* #36 (ΦΦΨ_z /ΦΦΨ_z)**

Atom	Wycoff	X	y	z
La/Sr	4a	¼ + x	¾ + y	0
La/Sr	8b	¼ + x	¼ + y	~ 0.31
Cr	8b	¾ + x	¼ + y	~ 0.4
O	8b	¼ + x	¾ + y	~ 0.7
O	4a	¾ + x	¼ + y	½
O	8b	x	½ + y	~ 0.1
O	8b	x	y	~ 0.1

***Pnam* #62 (ΦΦΨ_z /ΦΦ-Ψ_z)**

Atom	Wycoff	x	y	z
La/Sr	4c	¾ + x	y	¼
La/Sr	8d	¾ + x	y	~ 0.05
Cr	8d	¾ + x	y	~ 0.85
O	4c	¾ + x	½ + y	¼
O	8d	¾ + x	y	~ 0.95
O	8d	x	¼ + y	~ 0.85
O	8d	½ + x	¼ + y	~ 0.35

***A2/a* #15 (ΦΦΦ$_z$ /ΦΦΦ$_z$)**

Atom	Wycoff	x	y	z
La/Sr	4e	¼	¼ + y	0
La/Sr	8f	¼ + x	¾ + y	~ 0.18
Cr	8f	¼ + x	¼ + y	~ 0.09
O	4e	¼	¼ + y	0
O	8f	x	y	~ 0.09
O	8f	½ + x	½ + y	~ 0.09
O	8f	¼ + x	¼ + y	~ 0.19

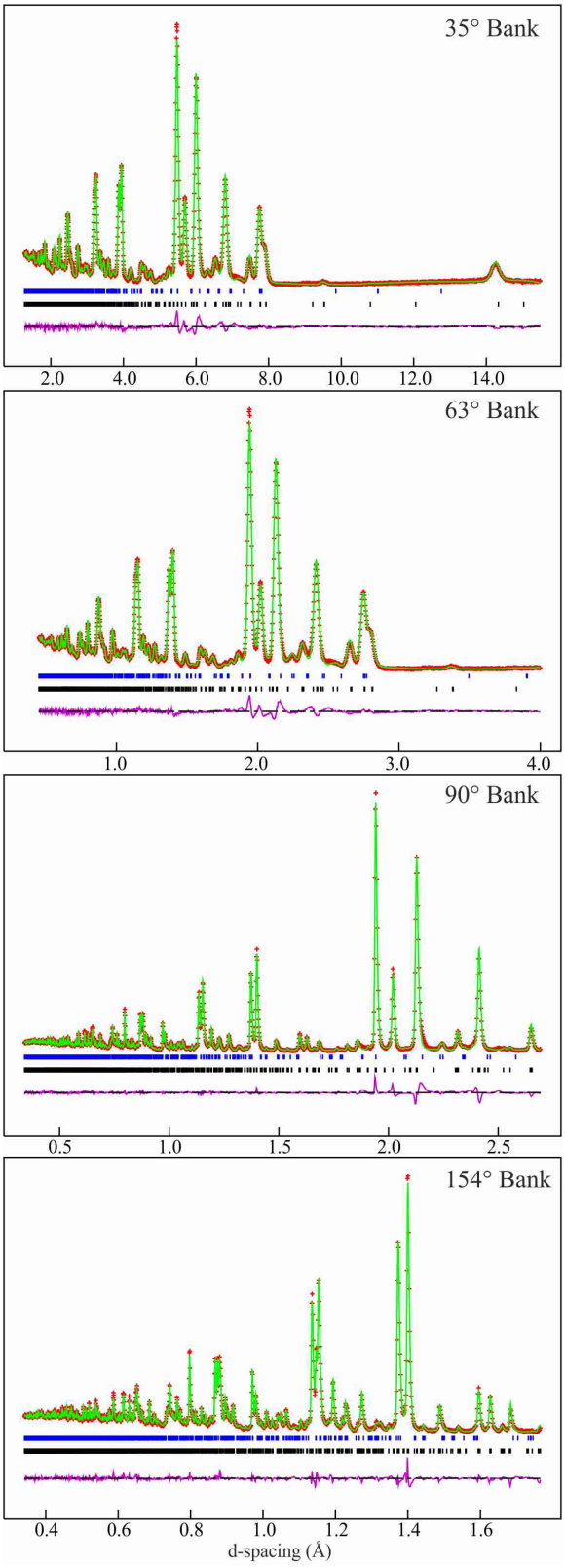

Figure S1. Observed, calculated and difference plots from the structural refinement of $La_2SrCr_2O_7$ against neutron powder diffraction data collected at room temperature. Lower tick marks indicate peak positions for the majority phase, upper tick marks for the $LaCrO_3$ secondary phase.

Cation	Anion	Bond length (Å)
La/Sr(1)	O(1)	2.754(1) × 2
	O(1)	2.856(8)
	O(1)	2.624(1)
	O(2)	2.862(9) × 2
	O(2)	2.807(9) × 2
	O(3)	2.674(8) × 2
	O(3)	2.653(8) × 2
La/Sr(2)	O(2)	2.562(9)
	O(2)	2.522(9)
	O(3)	2.671(8)
	O(3)	2.629(8)
	O(4)	2.786(8)
	O(4)	2.849(5)
	O(4)	2.747(8)
	O(4)	2.671(5)
	O(4)	2.423(2)
Cr(1)	O(1)	1.972(2)
	O(2)	2.000(13)
	O(2)	1.876(13)
	O(3)	1.919(12)
	O(3)	1.973(12)
	O(4)	2.037(3)
Cr(1)-O(1)-Cr(1)	170.88(8)	
Cr(1)-O(2)-Cr(1)	175.08(55)	
Cr(1)-O(3)-Cr(1)	173.68(51)	

Table S1. Selected bond lengths from the refined structure of $La_2SrCr_2O_7$ at 298K.

2. A-Cation Displacements in $La_2SrCr_2O_7$ Structural Models

As noted in the main text the cooperative twisting of the CrO_6 octahedra is driven by the need to satisfy the local bonding requirements of the relatively small La/Sr A-cation site. The cooperative rotations of the CrO_6 octahedra make the 9- and 12-coordinate A-cations sites 'smaller' and in the process lower the point symmetry of the A-sites, driving the A-cations to move from the original high-symmetry positions to better satisfy their bonding requirements. Figure S1 shows these A-cation displacements in the structures refined for $La_2SrCr_2O_7$ in spacegroups $A2_1am$ and A2/a.

$A2_1am$ model: It can be seen that both the 12-coordinate La/Sr(1) A-site and the 9-coordinate La/Sr(2) A-site are displaced in the same direction, predominantly along the a-axis. This displacement of the La/Sr(1) and La/Sr(2) sites is not chemically realistic – we would expect the two sites to be displaced in opposite directions to maximize the bonding requirements of the A-cations. This can most easily be seen by observing that the ($\Phi\Phi\Psi_z$ /$\Phi\Phi\Psi_z$) twisting distortion of the $A2_1am$ model is the same as that of the $GdFeO_3$ perovskite structure (space group Pnma) in which alternate sheets of 12-coordinate A-cations are displaced in alternate directions. Thus we can see that the refined structure of $La_2SrCr_2O_7$ is not chemically realistic and should be rejected.

A2/a model: As well as giving the best statistical fit to the data, the model in space group A2/a is the only one of the 'three twist' distortion models to refine to give a chemically and physically reasonable structure, with the combination of A-cation displacements expected for the observed octahedral rotation pattern.

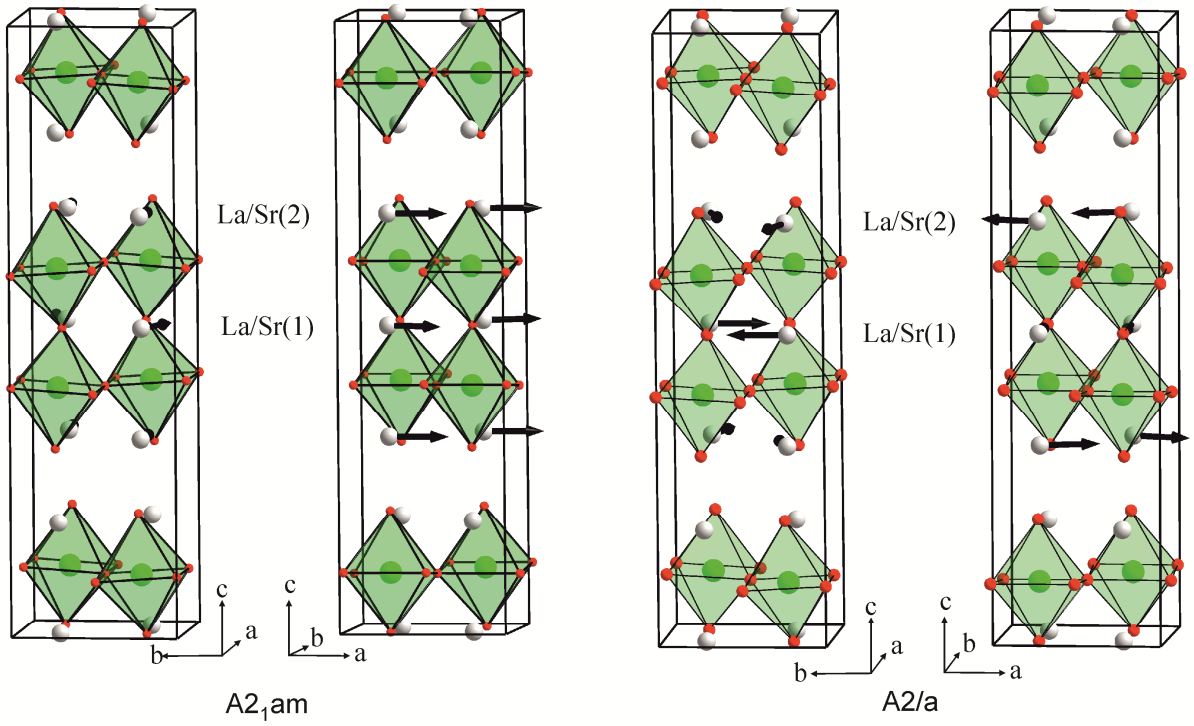

Figure S2. Structures of $La_2SrCr_2O_7$ refined in space groups $A2_1am$ and A2/a. Arrows indicate the displacement of the (La/Sr) A-cation sites from the high symmetry positions.

3. Magnetic Symmetry Analysis

The analysis of the magnetic symmetry of $La_2SrCr_2O_7$ in space group A2/a yielded the following 4 irreducible representations. Note the A-centring of the unit cell.

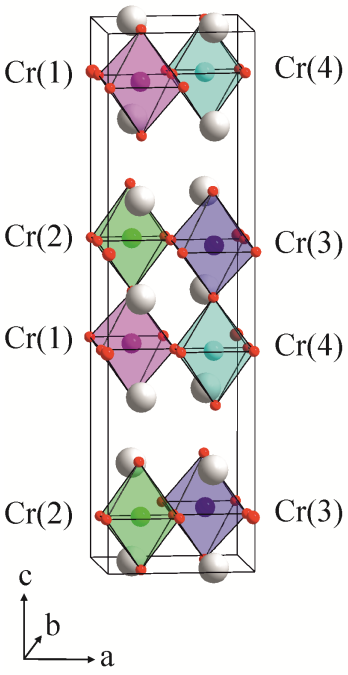

Irreducible Representation 1

Shubnikov Group: A2/a

Basis Vector 1			
Atom	x	y	z
Cr(1)	0	0	1
Cr(2)	0	0	-1
Cr(3)	0	0	1
Cr(4)	0	0	-1
Basis Vector 2			
Atom	x	y	z
Cr(1)	0	1	0
Cr(2)	0	1	0
Cr(3)	0	1	0
Cr(4)	0	1	0
Basis Vector 3			
Atom	x	y	z
Cr(1)	1	0	0
Cr(2)	-1	0	0
Cr(3)	1	0	0
Cr(4)	-1	0	0

Irreducible Representation 2

Shubnikov Group: A2/a’

Basis Vector 1			
Atom	x	y	z
Cr(1)	0	0	1
Cr(2)	0	0	-1
Cr(3)	0	0	-1
Cr(4)	0	0	1
Basis Vector 2			
Atom	x	y	z
Cr(1)	0	1	0
Cr(2)	0	1	0
Cr(3)	0	-1	0
Cr(4)	0	-1	0
Basis Vector 3			
Atom	x	y	z
Cr(1)	1	0	0
Cr(2)	-1	0	0
Cr(3)	-1	0	0
Cr(4)	1	0	0

Irreducible Representation 3

Shubnikov Group: A2’/a’

Basis Vector 1			
Atom	x	y	z
Cr(1)	0	0	1
Cr(2)	0	0	1
Cr(3)	0	0	1
Cr(4)	0	0	1
Basis Vector 2			
Atom	x	y	z
Cr(1)	0	1	0
Cr(2)	0	-1	0
Cr(3)	0	1	0
Cr(4)	0	-1	0
Basis Vector 3			
Atom	x	y	z
Cr(1)	1	0	0
Cr(2)	1	0	0
Cr(3)	1	0	0
Cr(4)	1	0	0

Irreducible Representation 4

Shubnikov Group: A2’/a

Basis Vector 1			
Atom	x	y	z
Cr(1)	0	0	1
Cr(2)	0	0	1
Cr(3)	0	0	-1
Cr(4)	0	0	-1
Basis Vector 2			
Atom	x	y	Z
Cr(1)	0	1	0
Cr(2)	0	-1	0
Cr(3)	0	-1	0
Cr(4)	0	1	0
Basis Vector 3			
Atom	x	y	z
Cr(1)	1	0	0
Cr(2)	1	0	0
Cr(3)	-1	0	0
Cr(4)	-1	0	0

4. Magnetic refinement details

Atom	site	*x*	*y*	*z*	Fraction	U_{iso} (Å^2)
La/Sr(1)	4e	¼	0.7437(8)	0	82/17	0.0063(1)
La/Sr(2)	8f	0.2444(8)	0.7465(5)	0.1817(1)	58/42	0.0051(2)
Cr(1)	8f	0.2516(15)	0.2490(14)	0.0978(1)	1	0.0011(2)
O(1)	4e	¼	0.2298(12)	0	1	0.0086(3)
O(2)	8f	0.9868(10)	0.9985(25)	0.1012(1)	1	0.0084(2)
O(3)	8f	0.5045(9)	0.5025(22)	0.0919(1)	1	0.0093(1)
O(4)	8f	0.2419(13)	0.2655(8)	0.1984(1)	1	0.0088(3)
$La_2SrCr_2O_7$ – space group: *A*2/*a* *a* = 5.4892(3) Å, *b* = 5.4765(3) Å, *c* = 20.157(1) Å, β = 89.88(1)º volume = 605.9(1)Å^3 phase fraction = 96.3 weight percent						
Atom		*x*	*y*	*z*	M_y (μ_B)	
Cr(1)		0.251	0.249	0.097	-2.51(3)	
Cr(2)		0.251	0.749	0.597	-2.51(3)	
Cr(3)		0.248	0.249	0.902	2.51(3)	
Cr(4)		0.248	0.749	0.402	2.51(3)	
Cr(5)		0.748	0.751	0.902	-2.51(3)	
Cr(6)		0.748	0.251	0.402	-2.51(3)	
Cr(7)		0.751	0.751	0.097	2.51(3)	
Cr(8)		0.751	0.251	0.597	2.51(3)	
$LaCrO_3$ – space group: Pnma *a* = 5.467(2) Å, *b* = 7.760(5) Å, *c* = 5.508(2) Å phase fraction = 3.7 weight percent						
χ^2 = 4.69, wRp = 4.24%, Rp = 3.11%						

Table S2. Nuclear and magnetic structural parameters refined against neutron powder diffraction data collected at 5 K from $La_2SrCr_2O_7$.

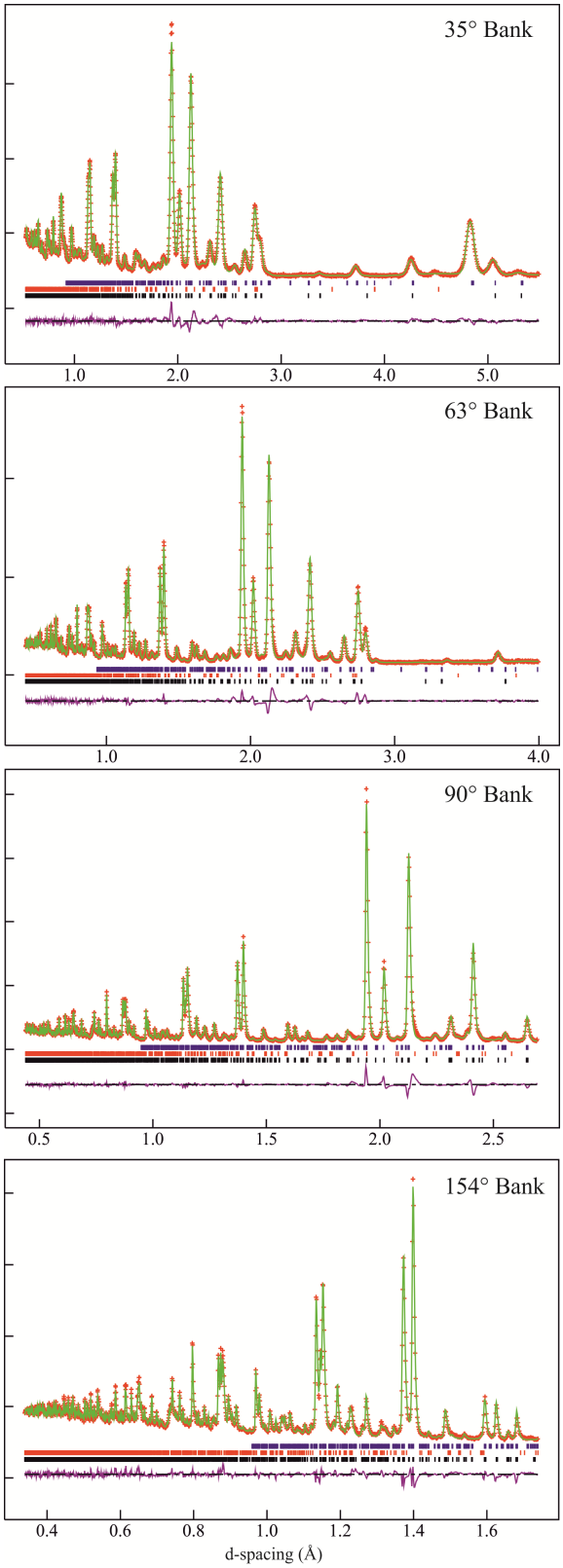

Figure S3. Observed, calculated and difference plots from the structural refinement of $La_2SrCr_2O_7$ against neutron powder diffraction data collected at 5K. Lower tick marks indicate nuclear peak positions for the majority phase, middle tick marks for the $LaCrO_3$ secondary phase, upper tick marks magnetic peak positions for the majority phase.

5. μ⁺SR data

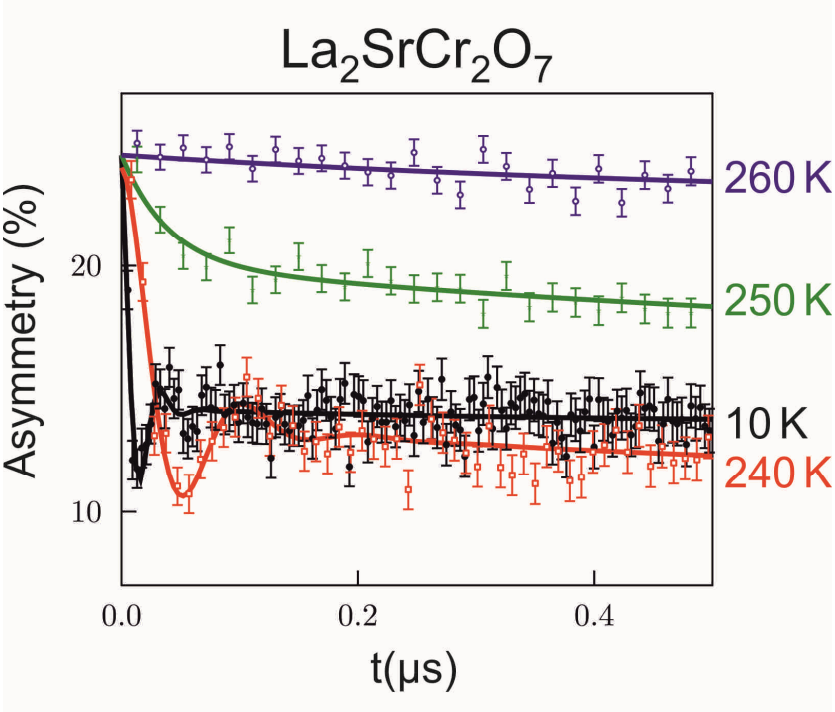

Figure S4. Oscillations in the asymmetry of μ⁺SR data collected from $La_2SrCr_2O_7$ at low temperature indicate long range magnetic order, consistent with the observation of antiferromagnetic order in the phase via neutron powder diffraction.

5. First principles structures

Table S3 enumerates the symmetry of each structure we considered. The La/Sr sites columns denote which La and Sr ions were swapped from their expected positions as shown in Figure S5. As an example the ninth row of Table S3 means that La4 and La8 sites were swapped with the Sr1 and Sr2 sites. The energies of these structures after relaxation is shown in Figure S6 as a function of the mean Sr-Sr distance in the relaxed *Amam* structure after swapping La/Sr for each A-site distribution.

Structure Number	La sites	Sr sites	*A2/a* like structure	*Pnam* like structure	*A2$_1$am* like structure
1	1	4	*P1*	*P1*	*P1*
2	1	3	*P1*	*P1*	*P1*
3	1	2	*P1*	*P1*	*P1*
4	1	1	*P1*	*P1*	*P1*
5	1, 2	3, 4	*P-1*	*P2$_1$*	*P1*
6	1, 7	1, 2	*P1*	*P1*	*P1*
7	1, 6	1, 2	*P1*	*P1*	*P1*
8	1, 4	1, 2	*Pc*	*Pc*	*Pc*
9	4, 8	1, 2	*P1*	*P1*	*P1*
10	1, 4	1, 3	*P1*	*P1*	*P1*
11	1, 3	1, 2	*P2*	*Pm*	*P1*
12	1, 7	1, 3	*P2$_1$*	*P2$_1$*	*Pc*
13	1, 2	1, 2	*P-1*	*P2$_1$*	*P1*
14	3, 4	1, 2	*P-1*	*P2$_1$*	*P1*
15	1, 2	1, 3	*P1*	*P1*	*P1*
16	1, 2	1, 4	*P1*	*P1*	*P1*
17	1, 3	1, 4	*P2*	*Pm*	*P1*
18	1, 3	1, 3	*P2*	*Pm*	*P1*
19	4, 8	2, 4	*P1*	*Pc*	*P1*
20	1, 4, 7	1, 2, 4	*P1*	*P1*	*P1*
21	1, 4, 7	1, 2, 3	*P1*	*P1*	*P1*
22	1, 7, 8	1, 2, 4	*P1*	*P1*	*P1*
23	1, 7, 8	1, 2, 3	*P1*	*P1*	*P1*
24	1, 7, 8	2, 3, 4	*P1*	*P1*	*P1*
25	3, 4, 8	1, 2, 3	*P1*	*P1*	*P1*
26	1, 4, 8	1, 3, 4	*P1*	*P1*	*P1*
27	1, 4, 8	2, 3, 4	*P1*	*P1*	*P1*
28	1, 7, 8	1, 3, 4	*P1*	*P1*	*P1*
29	3, 4, 8	1, 2, 4	*P1*	*P1*	*P1*
30	1, 4, 8	1, 2, 3	*P1*	*P1*	*P1*
31	1, 4, 8	1, 2, 4	*P1*	*P1*	*P1*
32	1, 4, 6, 7	1, 2, 3, 4	*P2$_1$/c*	*P2$_1$/c*	*Pca2$_1$*
33	1, 4, 7, 8	1, 2, 3, 4	*P1*	*P1*	*P1*
34	3, 4, 5, 6	1, 2, 3, 4	*P2$_1$/c*	*P2$_1$2$_1$2$_1$*	*Pc*
35	3, 4, 7, 8	1, 2, 3, 4	*P-1*	*P2$_1$/c*	*P2$_1$*
36	1, 4, 5, 8	1, 2, 3, 4	*Cc*	*Pna2$_1$*	*Pc*

Table S3. Symmetries of the structures we considered with alternate A-site orders. Refer to Figure S5. For labelling scheme of the La and Sr sites.

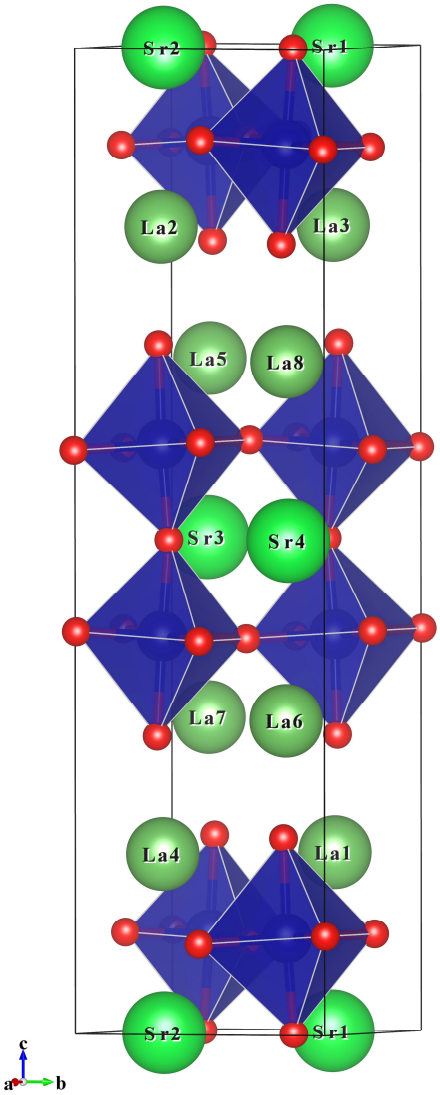

Figure S5. Schematic labelling the A-site positions.

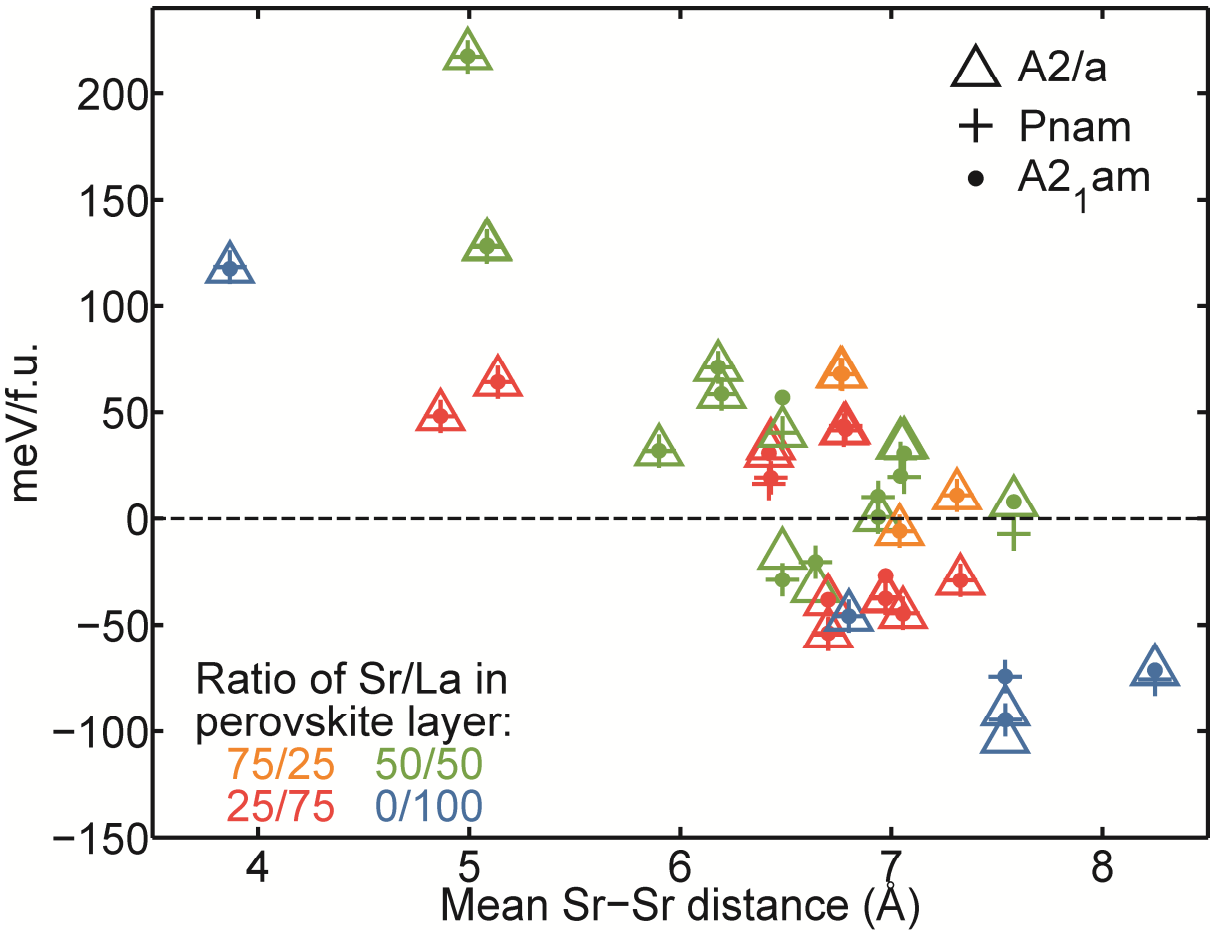

Figure S6. Relaxed energies per formula unit (f.u.) of our 108 structures with varying La/Sr distributions with respect to the energy of the *Amam* reference structure with La/Sr cations on their expected sites (we take the energy of this structure to be the zero of energy, indicated by the horizontal dashed line). Color and shape of points indicate the ratio of Sr/La distribution and initial ionic positions respectively. The horizontal axis is the mean distance between Sr cations in our relaxed *Amam* structure after swapping Sr/La positions, but before any further relaxation.

6. Magnetic ordering in first principles calculations

To check the effect of magnetic ordering on our simulations, we calculated the energies for each of our relaxed structures with the observed experimental antiferromagnetic ordering. The energy of the antiferromagnetic energy is lower for each structure, but the energy drop is similar for each structure. Figure S6 shows the energies of our structures with both ferromagnetic and antiferromagnetic ordering. The relative energy difference between structures is qualitatively similar for each magnetic ordering so the trends we found with ferromagnetic ordering should also exist in structures with antiferromagnetic ordering.

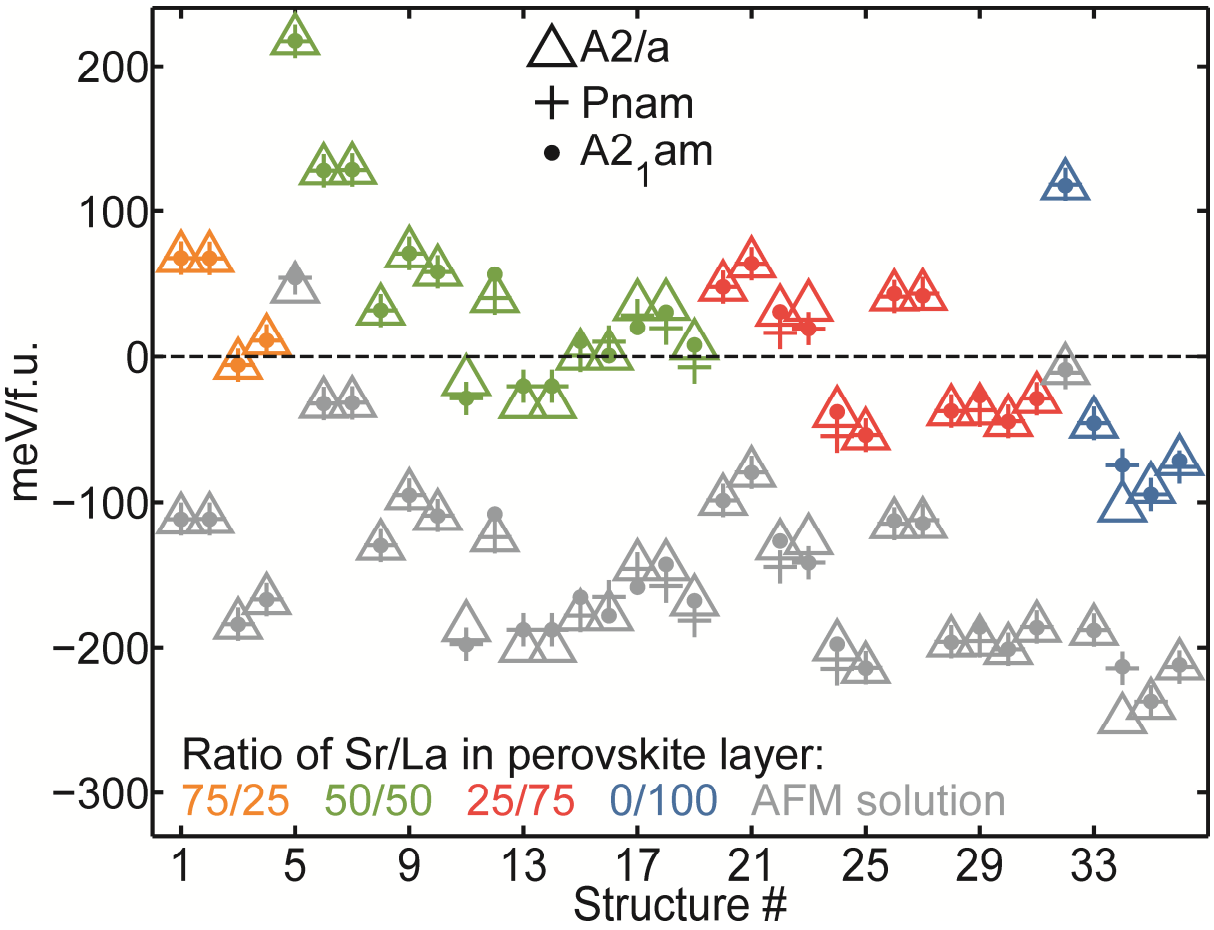

Figure S7. Calculated energies of our relaxed structures. The zero of energy is taken as the energy of the *Amam* structure with ferromagnetic spin ordering. Colored points have ferromagnetic ordering, while the corresponding gray point is the energy of the same structure with antiferromagnetic ordering.

7. Linear correlation analysis of structural features

To guide our search for structural trends we calculated statistical quantities for a range of structural features for each of our relaxed structures, as listed in Table S4. Many of these features are based on the bond valence model. In many cases we averaged a particular feature over the entire structure, which was necessary because the low symmetry of many structures allowed, for instance, each CrO_6 octahedron in a particular structure to be unique. We also included variances, minima, and maxima of various structural features to help quantify structures with a large range of a particular structural feature.

After calculating each of the features in Table S4 we calculated a pairwise linear correlation coefficient for each pair of features within each of the structures we considered. Figure S7 is a visualization of the results for structures relaxed starting from the *A2/a* ionic positions and constrained to the experimental unit cell. This allowed us to easily identify trends, such as the nearly perfect correlation between the average maximum Cr-O bond length and the average CrO_6 volume.

For comparison we also show the pairwise linear correlation coefficients for relaxations starting from the *A2/a* ionic positions but with an unconstrained unit cell in Figure S8. While the overall trends

appear similar, the structural correlations after allowing cell relaxation tend to be weaker. This is especially apparent for features involving average discrepancy factors (features 28-36). We attribute this difference in part to the low symmetry of our structures, which allows the unit cell to relax in a different way for each structure. Further, the bond valence model is based on coefficients that are fit to experimental data. In our experience this seems to cause the model to become less reliable for interpreting DFT results that are not constrained to the experimental volume. For these reasons, we focused on results that were constrained to the experimental unit cell.

1	Calculated energy of structure
2	Average Cr-O-Cr in plane angle
3	Variance of Cr-O-Cr in plane angle
4	Average Cr-O-Cr angle
5	Variance of Cr-O-Cr angle
6	Bond valence global instability index
7	Average Cr-O bond length
8	Average CrO_6 volume
9	Average CrO_6 distortion index
10	Average CrO_6 quadratic elongation
11	Average CrO_6 bond angle variance
12	Variance of the average Cr-O bond length in each CrO_6
13	Variance of CrO_6 volumes
14	Variance of CrO_6 distortion indices
15	Variance of CrO_6 quadratic elongations
16	Variance of CrO_6 bond angle variance
17	Minimum of average Cr-O bond length in each CrO_6
18	Minimum CrO_6 volume
19	Minimum CrO_6 distortion index
20	Minimum CrO_6 quadratic elongation
21	Minimum CrO_6 bond angle variance
22	Maximum of average Cr-O bond length in each CrO_6
23	Maximum CrO_6 volume
24	Maximum CrO_6 distortion index
25	Maximum CrO_6 quadratic elongation
26	Maximum CrO_6 bond angle variance
27	Range of CrO_6 distortion indices
28	Average discrepancy factor of La
29	Average discrepancy factor of Sr
30	Average discrepancy factor of Cr
31	Average discrepancy factor of La in perovskite layer

32	Average discrepancy factor of La in rock salt layer
33	Average discrepancy factor of Sr in rock salt layer
34	Average discrepancy factor of apical oxygen in perovskite layer
35	Average discrepancy factor of apical oxygen in rock salt layer
36	Average discrepancy factor of equatorial oxygen
37	Variance of discrepancy factor of La
38	Variance of discrepancy factor of Sr
39	Variance of discrepancy factor of CR
40	Variance of discrepancy factor of La in perovskite layer
41	Variance of discrepancy factor of La in rock salt layer
42	Variance of discrepancy factor of Sr in rock salt layer
43	Variance of discrepancy factor of apical oxygen in perovskite layer
44	Variance of discrepancy factor of apical oxygen in rock salt layer
45	Variance of discrepancy factor of equatorial oxygen
46	Ratio of Sr in perovskite layer
47	Average minimum Cr-O bond length
48	Average maximum Cr-O bond length

Table S4. List of the structural features we calculated for each of our relaxed structures.

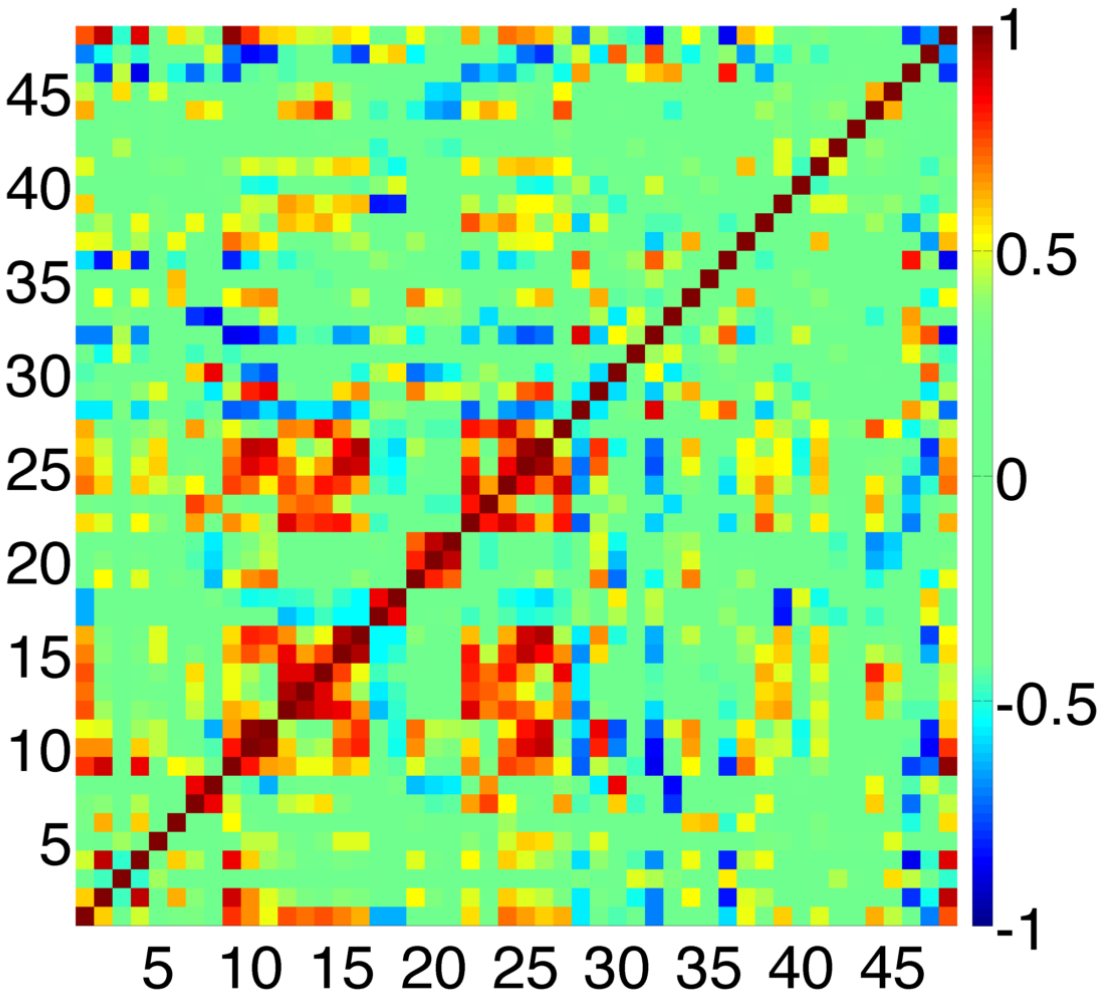

Figure S8. Linear correlation coefficients of the features listed in Table S4 for structures relaxed starting from *A2/a* ionic positions and constrained to the experimental unit cell.

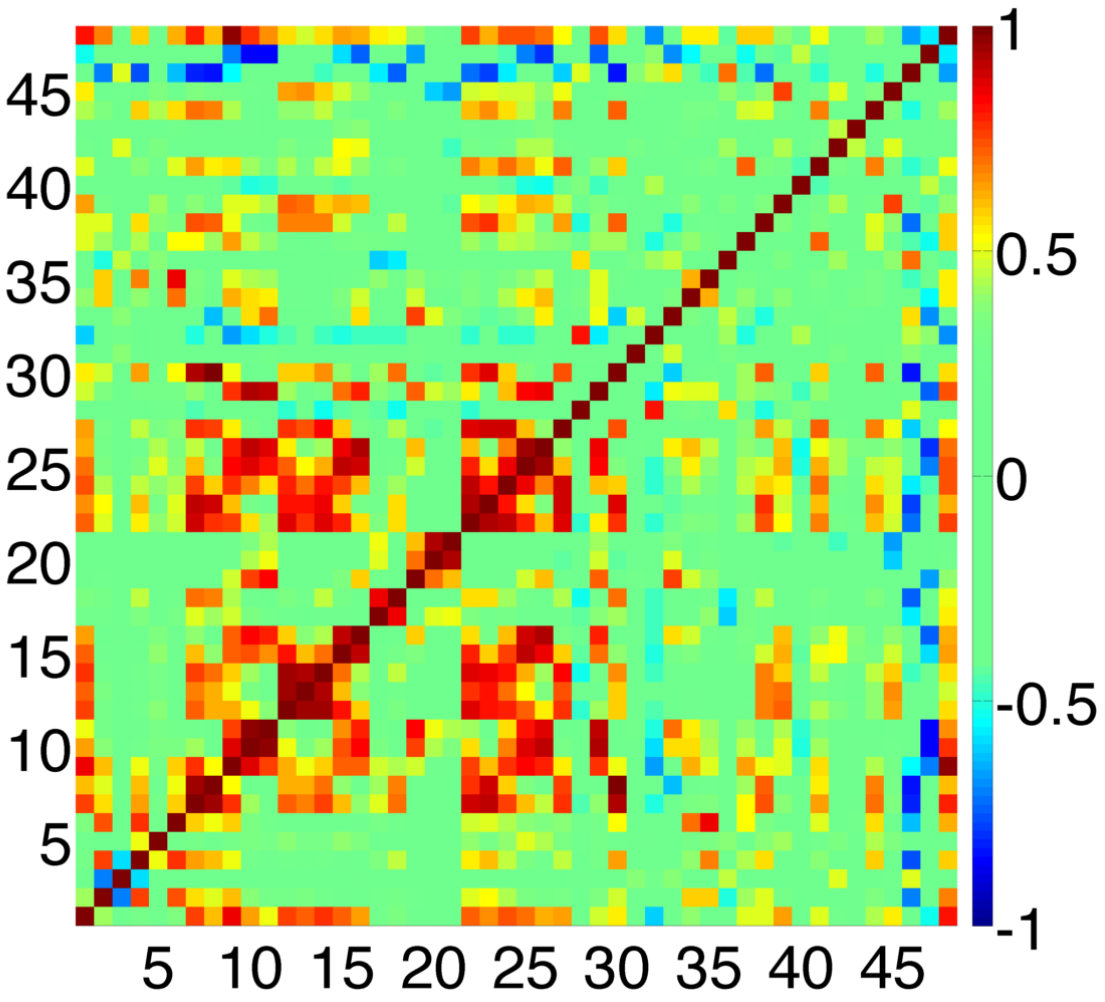

Figure S9. Linear correlation coefficients of the features listed in Table S4 for structures relaxed starting from *A2/a* ionic positions with the unit cell fully relaxed.